2018

Axial and flexural behaviour of circular reinforced concrete columns strengthened with reactive powder concrete jacket and fibre reinforced polymer wrapping

Muhammad N. S Hadi
University of Wollongong, mhadi@uow.edu.au

Atheer Hilal Mahdi Al - Gburi
University of Wollongong, ahmag930@uowmail.edu.au

M Neaz Sheikh
University of Wollongong, msheikh@uow.edu.au

Allister T. Carrigan
University of Wollongong, atc277@uowmail.edu.au

Recommended Citation

Axial and flexural behaviour of circular reinforced concrete columns strengthened with reactive powder concrete jacket and fibre reinforced polymer wrapping

Abstract

This paper investigates axial and flexural behaviour of circular reinforced concrete (RC) columns strengthened with reactive powder concrete (RPC) jacket and fibre reinforced polymer wrapping. The experimental results of 16 circular RC column specimens have been presented. The specimens were divided into four groups of four specimens. Column specimens of the first group were the reference RC specimens without any strengthening, specimens of the second group were strengthened by wrapping with two layers of carbon fibre reinforced polymer (CFRP), specimens of the third group were jacketed with a 25 mm thick layer of RPC and specimens of the fourth group were jacketed with a 25 mm thick layer of RPC then wrapped with a single layer of CFRP. Test results demonstrated that jacketing with a thin layer of the RPC enhanced significantly the ultimate axial and flexural loads as well as energy absorption of circular RC column specimens. Wrapping the RPC jacketed specimens with CFRP improved the ultimate axial load, ductility and energy absorption of the specimens.

Disciplines

Engineering | Science and Technology Studies

Publication Details

Axial and Flexural Behaviour of Circular Reinforced Concrete Columns

Strengthened with Reactive Powder Concrete Jacket and Fibre Reinforced

Polymer Wrapping

Muhammad N.S. Hadi [1*]

[1]Associate Professor, School of Civil, Mining and Environmental Engineering, University of Wollongong, NSW 2522, Australia, [*]Corresponding Author, Email: mhadi@uow.edu.au,. Tel.: +61 2 4221 4762; Fax: +61 2 4221 3238.

Atheer H.M. Algburi [2]

[2]Ph.D. Candidate, School of Civil, Mining and Environmental Engineering, University of Wollongong, NSW 2522, Australia. E-mail: ahmag930@uowmail.edu.au

M. Neaz Sheikh [3]

[3]Associate Professor, School of Civil, Mining and Environmental Engineering, University of Wollongong, NSW 2522, Australia. E-mail: msheikh@uow.edu.au

Allister T. Carrigan[4]

[4]Formely BE student at University of Wollongong, Australia. Email atc277@uowmail.edu.au

Abstract

This paper investigates axial and flexural behaviour of circular reinforced concrete (RC) columns strengthened with reactive powder concrete (RPC) jacket and fibre reinforced polymer wrapping. The experimental results of 16 circular RC column specimens have been presented. The specimens were divided into four groups of four specimens. Column specimens of the first group were the reference RC specimens without any strengthening, specimens of the second group

24 were strengthened by wrapping with two layers of carbon fibre reinforced polymer (CFRP),

25 specimens of the third group were jacketed with a 25 mm thick layer of RPC and specimens of

26 the fourth group were jacketed with a 25 mm thick layer of RPC then wrapped with a single

27 layer of CFRP. Test results demonstrated that jacketing with a thin layer of the RPC enhanced

28 significantly the ultimate axial and flexural loads as well as energy absorption of circular RC

29 column specimens. Wrapping the RPC jacketed specimens with CFRP improved the ultimate

30 axial load, ductility and energy absorption of the specimens.

31

32 Keywords: Concrete columns; Reactive powder concrete; FRP; Jacketing; Wrapping.

33

34 **1. Introduction**

35 Reinforced concrete (RC) columns in buildings, highway bridges and other infrastructure may

36 need to be strengthened in some cases. These cases include deterioration due to corrosion of steel

37 reinforcement, damage after an earthquake event, inadequate design, functional changes and

38 construction errors. Deficient RC columns have to be repaired before strengthening [1].

39 Jacketing is one of the most practical techniques used for restoring deficient RC columns [2].

40 The traditional reinforced concrete jacket probably no longer remains an effective jacketing

41 technique as it is associated with several disadvantages including decrease in the available space

42 of the strengthened structure, a significant increase of the dead load, slow construction process

43 and practical problems for the required dowelling with the existing column as well as with the

44 slab and foundation [1, 3, 4].

45

46   The other commonly used jackets for increasing the axial strength of RC columns are steel and

47   fibre reinforced polymer (FRP) jackets [5]. Steel jacket has the problem of low corrosion

48   resistance [6]. Hence, FRP is considered as one of the most suitable jacketing materials for

49   strengthening RC columns. The FRP has a higher strength to weight ratio and superior durability

50   compared to steel [7]. Wrapping RC columns with FRP increases the strength and ductility of the

51   RC columns. However, FRP wrapping cannot be applied directly for strengthening a deteriorated

52   RC column unless the surface of the RC column is suitably repaired. Also, the reliability of FRP

53   wrapping decreases under freezing, thawing and temperature changes [8].

54

55   Similar to steel jacket, FRP jacket depends mainly on the principle of the lateral confinement

56   pressure [6]. The efficiency of the confinement decreases when a column is subjected to an

57   eccentric axial load [9-11]. Also, the confinement effect decreases when the diameter of the

58   cylindrical concrete specimens increases [12]. Thus, several layers of FRP are required if only

59   FRP wrapping is used for the strengthening of large diameter RC columns. Increasing the FRP

60   layers is not only expensive but also causes bond failure [8]. Moreover, only slight improvement

61   in the yield strength and flexural capacity of the RC column can be achieved by the FRP

62   wrapping [13].

63

64   Reactive powder concrete (RPC) is a high performance concrete with high strength and high

65   ductility [14]. The RPC has a dense structure, which is formed mainly by cement, silica fume,

66   fine aggregate, water and superplasticizer. Steel fibre is usually used to improve the ductility of

67   the RPC. The absence of the coarse aggregate in the RPC matrix is the main difference between

68   the RPC and the other types of concrete. The high strength of the RPC reduces the required

69 reinforcement and cross-sectional dimensions for the RPC structural members compared to the

70 conventional RC members [15]. Lee et al. [16] and Chang et al. [17] proposed using the RPC as

71 a durable strengthening and repairing material. Lee et al. [16] and Chang et al. [17] used the RPC

72 to strengthen cylinder and prism specimens exposed to hazardous conditions to increase the

73 compressive and flexural strength of the specimens.

74

75 Even though RPC has a superior compressive strength compared to other types of concrete,

76 studies on the use of RPC in the columns are still very limited. Malik and Foster [18] however,

77 conducted an experimental study on circular RPC column specimens wrapped with carbon fibre

78 reinforced polymer (CFRP). The study reported that the axial strength of the CFRP confined

79 RPC column specimen was 19% higher than the axial strength of unconfined column specimen.

80 Also, Huynh et al. [19] examined the behaviour of square RC specimens constructed of high

81 strength concrete (HSC) and RPC under three-point bending. The test results indicated that the

82 partial replacement of the HSC by the RPC enhanced the strength and energy absorption capacity

83 of the tested specimens. However, strengthening of RC columns with RPC jacket has not been

84 investigated yet. This study proposes using RPC jacket for strengthening existing deficient

85 circular RC columns.

86

87 The objective of this study is to develop an effective strengthening technique with RPC jacket

88 and FRP wrapping for the existing deficient circular RC columns. The experimental

89 investigation results of circular RC column specimens strengthened with a thin layer of RPC

90 jacket and wrapped with FRP tested under different loading conditions have been presented. The

91 loading conditions included concentric axial load, eccentric axial loads and four-point bending.

92   The innovating strengthening technique of using RPC jacket and FRP wrapping has been found

93   to be effective in increasing the yield load, ultimate load and energy absorption capacity of

94   existing deficient circular RC columns.

95

96   **2. Experimental program**

97   *2.1. Test matrix*

98   The experimental program of this study included preparing and testing of 16 RC column

99   specimens. These specimens were divided into four groups of four specimens based on the

100 adopted strengthening technique. All base specimens (assumed to be existing columns) had a

101 diameter of 150 mm with a height of 800 mm. Each base specimen was reinforced longitudinally

102 with 6N10 (6 deformed steel bars of 10 mm diameter) and transversely with R6 (smooth steel bar

103 of 6 mm diameter) helices at a centre to centre spacing of 50 mm. A clear concrete cover of 15

104 mm was provided at the sides and at the top and bottom of the specimen. All base specimens

105 were cast with normal strength concrete (NSC) having a target compressive strength of 25 MPa.

106 The NSC was supplied by a local company. The first group was the reference RC base

107 specimens without any strengthening and was identified as Group C specimens. Specimens of

108 the second group were wrapped with two layers of CFRP and were identified as Group CF

109 specimens. The specimens of the third group were strengthened with a 25 mm thick RPC jacket

110 and were identified as Group CJ specimens. The thickness of 25 mm was chosen for RPC jacket

111 because the thickness of 25 mm was considered as the minimum practical thickness of the RPC

112 jacket for the ease of cast and compaction. The specimens of the last group were strengthened

113 with a 25 mm thick RPC jacket then wrapped with a single layer of CFRP. The specimens of the

114 last group were identified as Group CJF specimens. The plan views of the reference and the

115 strengthened specimens are shown in Fig. 1. From each group, one specimen was tested under

116 concentric axial load, two specimens were tested under 15 mm and 25 mm eccentric axial loads,

117 respectively, and the remaining specimen was tested under four-point bending. To identify the

118 loading condition, a number or a letter were added to the labels of the specimens. The first part

119 of each specimen label refers to the group name and the second part refers to the loading

120 condition. For instance, Specimen CF-25 refers to the specimen that was wrapped with two

121 layers of CFRP and tested under 25 mm eccentric axial load. Specimen CJ-B was jacketed with

122 25 mm thick RPC and tested under four-point bending. The details of the specimens are

123 presented in Table 1.

124

125 *2.2. Preparation of RPC*

126 Typical RPC mix usually includes cement, silica fume, fine sand, superplasticizer, water and

127 steel fibre. General Purpose cement (Type GP) according to AS 3972-2010 [20] was used to

128 prepare the RPC. Densified silica fume was used as a supplementary cementitious material. The

129 silica fume was produced in SIMCOA silicon plant, Western Australia [21], and was supplied by

130 Australasian (iron & steel) Slag Association [22]. The sand used for the RPC was washed fine

131 river sand with particle size ranging between 150 µm and 600 µm. Master Glenium SKY 8700

132 used as a superplasticizer, which was supplied by BASF, Australia [23]. The steel fibres used in

133 this study were straight and smooth with a length of 13 mm, a diameter of 0.2 mm, an aspect

134 ratio (length/diameter) of 65, a density of 7.8 g/cm^3 and a nominal tensile strength of 2500 MPa

135 [24]. The steel fibres are shown in Fig. 2. The steel fibres were supplied by Steel Wire Fibre in

136 China [24].

137

138   The RPC mix design is presented in Table 2. The proportion of the steel fibre was 1.5% by

139   volume. The proportion of steel fibre (1.5% by volume) was selected based on the experimental

140   findings in Ju et al. [25]. Mixing of RPC batches was carried out using a vertical pan mixer in the

141   Structural Engineering Laboratories at the University of Wollongong, Australia. Flow table test

142   according to ASTM C230-14 [26] was used to evaluate the flowability of the RPC. The produced

143   RPC achieved high flowability with 220 mm flow diameter.

144

145   *2.3. Properties of materials*

146   Engineering properties of the NSC and RPC were determined according to AS 1012-2014 [27-

147   29] except the shear strength of the RPC which was determined according to JSCE SF6-1999

148   [30]. The details of the specimens and tests results for the RPC at 28 days are shown in Table 3.

149   The average compressive strength of the RPC was 110 MPa at 28 days (start of the test) and 113

150   MPa at the end of the test. At age of 28 days, the average splitting tensile strength of the RPC

151   was 9 MPa. The splitting tensile test was used to determine the tensile strength of the RPC, as

152   recommended in AS 3600-2009 [31] for concrete. The average modulus of rupture of the RPC

153   was 12 MPa and the average shear strength was 30 MPa. The NSC had an average compressive

154   strength of 29 MPa and an average splitting tensile strength of 2.5 MPa at 28 days. The

155   compressive strength of the NSC was 33 MPa at the start of the test and 35 MPa at the end of the

156   test.

157

158   The tensile strength of both longitudinal and transverse steel reinforcement bars of the base

159   specimens was determined according to AS 1391-2007 [32] using the Instron 8033 testing

160   machine with a capacity of 500 kN. The deformed N10 steel bar had an average yield tensile

7

161 strength of 524 MPa and an average ultimate tensile strength of 660 MPa. The smooth R6 steel

162 bar had an average yield tensile strength of 578 MPa and an average ultimate tensile strength of

163 613 MPa. The CFRP sheet had an average width of 100 mm and an average thickness of 0.3 mm.

164 The coupon test according to ASTM D3039-08 [33] was used to determine the tensile strength of

165 the CFRP. The specimens of the coupon test had an average width of 25 mm and an average

166 length of 250 mm. The test was conducted using the Instron 8033 testing machine with a

167 capacity of 500 kN. The average maximum tensile force per unit width of one layer of the CFRP

168 sheet was 537 N/mm. The average maximum tensile force per unit width of two layers of the

169 CFRP sheets was 1249 N/mm. Test results of the CFRP with one and two layers are reported in

170 Table 4.

171

172 *2.4. Preparation of test specimens*

173 Formwork of the base specimens was prepared by using PVC pipes with a clear interior diameter

174 of 150 mm and a height of 800 mm. The PVC pipes were supported by plywood frames at the

175 top and the bottom. The bottoms of the PVC pipes were fixed with a plywood base by silicon

176 glue. The longitudinal bars were cut and tied with the helix to form reinforcement cages. All

177 reinforcement cages were placed inside the formworks. The NSC was cast inside the formwork

178 then compacted using two small electric vibrators. The base specimens were left to cure for one

179 day then covered with wet hessian rugs for six days. The base specimens were demoulded after

180 seven days of the wet curing then left to cure under the laboratory conditions until the day of the

181 RPC jacketing (26-day age). Eight base specimens were jacketed with RPC (Groups CJ and CJF)

182 and the remaining eight specimens were left without jacketing. Later, four of the unjacketed

183   specimens were wrapped with two layers of CFRP (Group CF) and the remaining four specimens

184   were left without any wrapping as reference specimens (Group C).

185

186   During the curing period of the base specimens, surface preparation and the formwork of the

187   RPC jacket for eight base specimens (Groups CJ and CJF) were completed. To ensure sufficient

188   bond strength between the surface of the base specimen and the RPC jacket, adequate care was

189   taken to make the surface of the base specimen rough. At first, the base specimen was

190   sandblasted inside a closed sandblasting chamber. Afterwards, a small chipping hammer was

191   used to prickle the zones of the base specimen which were not adequately sandblasted (Fig. 3).

192   Then, a steel wire brush was used to remove all the weak particles from the surface of the base

193   specimen. The specimens were then cleaned by an air jet. At last, the surface of the base

194   specimen was cleaned with a piece of wet cloth and left to dry in the laboratory.

195

196   The formwork of the RPC jacket was prepared by using an easy form cardboard with a 200 mm

197   clear interior diameter. After the surface preparation was done, the eight base specimens were

198   placed on a plywood base then each cardboard formwork was installed on a specimen and glued

199   with the plywood base. The cardboard formwork was supported vertically by plywood frames at

200   the top, mid-height and bottom. The RPC jackets were then cast. Two small electric vibrators

201   were applied on the outer surface of the formwork to compact the RPC. The flowability of the

202   produced RPC was high enough to achieve an efficient pouring for the RPC between the

203   formwork and the base specimen. Figure 4 shows the formwork of the base and RPC jacketed

204   specimens before and after jacketing. The RPC jacketed specimens (Groups CJ and CJF) were

205   left to cure for one day then covered with wet hessian rugs for six days. Afterwards, the eight

9

206 jacketed specimens were demoulded. Four specimens (Group CJF) were prepared for wrapping

207 with CFRP.

208

209 The specimens of Groups CF and CJF were wrapped with CFRP sheets by the wet layup

210 technique. First, the CFRP sheets were cut into pieces of specified lengths equal to the specimen

211 circumference (or twice the specimen circumference in case of two layers wrapping) plus 100

212 mm for the circumferential overlap. The CFRP sheet was coated with epoxy resin on both sides.

213 The epoxy resin was prepared by mixing epoxy and hardener at a ratio of 5:1 by volume. The

214 specimen surface was also coated with the epoxy resin. The coated CFRP sheet was wrapped

215 gently on the surface of the specimen without adding any additional epoxy resin between the

216 layers. Lastly, the surface of the CFRP sheet was coated with a very thin layer of epoxy resin,

217 especially at the overlap zone. This technique was found to be effective in preventing de-bonding

218 failure between the CFRP layers during testing. The CFRP sheets were wrapped with a vertical

219 overlap of 10 mm. The specimens of Groups CF and CJF were wrapped entirely with CFRP.

220 Specimens of Group CF were wrapped with two layers of CFRP, whereas the Specimens of

221 Group CJF were wrapped with one layer of CFRP.

222

223 All specimens which were tested under the concentric and eccentric axial loads were wrapped at

224 the ends with two layers of CFRP of 100 mm wide to prevent any premature failure at the ends

225 of the specimen during testing. The four specimens which were tested under four-point bending

226 were wrapped with two layers of CFRP from the two ends up to the mid one-third (up to the pure

227 bending moment zone) of the specimen. This was done to avoid shear failure for Specimen CJ-B.

228   The same wet layup technique was used to wrap the ends of the specimens. All wrapped

229   specimens were left to cure in the laboratory for at least seven days before testing.

230

231   *2.5. Instrumentation and test procedure*

232   All reference and strengthened RC specimens were tested using the Denison testing machine

233   with a capacity of 5000 kN under displacement control load application at 0.5 mm per minute.

234   The data of the axial load were captured directly from load cell of the testing machine, while the

235   data of the axial deformation were recorded from average readings of two Linear Variable

236   Differential Transducers (LVDTs). The two LVDTs were connected with the lower plate of the

237   test machine and attached vertically with the two opposite corners of the upper plate of the test

238   machine. The mid-height lateral deformation of the eccentrically loaded specimens and the

239   midspan deflection of the four-point bending test specimens were captured by a laser

240   triangulation. Loading heads similar to those used by Hadi et al. [34] were used to apply the

241   eccentric axial load. The specimens were capped at the top and bottom using high strength

242   plaster and left to dry for about one hour before the test. The test setup of the eccentrically

243   loaded specimen is shown in Fig. 5. The steel frame that was used for the four-point bending test

244   of Specimens CB, CFB, CJB and CJFB was similar to that used by Hadi et al. [35]. The shear

245   span provided for all the specimens tested under four-point bending was 233 mm.

246

247   **3. Results of testing**

248   *3.1 Definition of strengthening ratio, ductility and energy absorption ratio*

249   To investigate the influence of the proposed strengthening method, the strengthening ratio was

250   calculated at both yield and ultimate loads. The yield strengthening ratio was expressed as the

11

251   ratio of the yield load of the strengthened specimen to the yield load of the corresponding

252   reference specimen in Group C. The ultimate strengthening ratio was expressed as the ratio of

253   the ultimate load of the strengthened specimen to the ultimate load of the corresponding

254   reference specimen in Group C.

255

256   The ductility was calculated by dividing the deformation corresponding to the 85% of the peak

257   load in the descending part of the load-deformation curve by the deformation at yield load (δ_y)

258   [36]. The δ_y was determined by the intersection point of two straight lines. The first straight line

259   is the best-fit regression line to the linear segment of the load-deformation curve and the second

260   line is a horizontal straight line passing through the ultimate load [37].

261

262   Energy absorption was calculated as the area under the load-deformation curve. In this study,

263   energy absorption for the specimens tested under concentric and eccentric axial loads was

264   expressed as the area under the load-deformation curve at $3\delta_y$ [38]. However, energy absorption

265   at $3\delta_y$ for the specimens tested under four-point bending was considered misleading, because the

266   deflection $3\delta_y$ occurred at a flexural load before the specimen reached the ultimate flexural load.

267   Therefore, energy absorption of the specimens tested under four-point bending was expressed as

268   the area under the load-deflection curve up to $10.5\delta_y$ [38]. The energy absorption ratio was

269   expressed as the ratio of the energy absorption of the strengthened specimen to the energy

270   absorption of the corresponding reference specimen in Group C.

271

272   *3.2. Behaviour of the concentrically loaded specimens*

273   Figure 6 shows the axial load-axial deformation response of the reference specimen and the

274   strengthened specimens under concentric axial load. Specimen C-0 experienced premature

275   concrete cover spalling at the mid-height followed by large cracks at different locations in the

276   specimen. The premature concrete cover spalling was probably due to the relatively small pitch

277   of the transverse reinforcement, which formed a plane of separation between the concrete core

278   and the concrete cover. Final failure of Specimen C-0 occurred due to the buckling of the

279   longitudinal steel bars, as shown in Fig. 7. The yield axial load of Specimen C-0 was 536 kN and

280   the yield axial deformation was 2.9 mm (Table 5). Specimen C-0 achieved an ultimate axial load

281   of 615 kN. After the spalling of concrete cover, the confinement of the transverse reinforcement

282   was activated and the specimen carried the applied axial load with a ductility of 5.7. This high

283   ductility was due to the high yield strength and the relatively small pitch of the transverse

284   reinforcement which generated high confinement to the concrete core. However, this high

285   ductility may not be representative of the existing deteriorated RC columns. The energy

286   absorption of the specimen was 4297 kN.mm. The axial deformation at the final failure of

287   Specimen C-0 was 19 mm.

288

289   Specimen CF-0 failed suddenly by the rupture of the CFRP and by the crushing of concrete at

290   the mid-height segment of the specimen, as shown in Fig. 7. The ultimate axial load of 1245 kN

291   was achieved by a quasi-bilinear behaviour with an increase in the axial load with the increase in

292   the axial deformation (hardening response). Yield strengthening ratio of 1.33 and ultimate

293   strengthening ratio of 2.02 were achieved by Specimen CF-0 (Table 5). Specimen CF-0

294   demonstrated a lower ductility compared to Specimen C-0. The ductility of Specimen CF-0 was

13

295 4. However, the energy absorption ratio was 1.43. The lower ductility of Specimen CF-0

296 compared to that of Specimen C-0 was due to the sudden rupture of the CFRP and crushing of

297 concrete which caused the final failure of the specimen before the buckling of the longitudinal

298 steel bars at an axial deformation of 18 mm, which was only 5% lower than that of Specimen C-

299 0. No residual axial load capacity for the Specimen CF-0 was observed after the ultimate axial

300 load.

301

302 The failure of Specimen CJ-0 started with a vertical crack along the length of the specimen then

303 inclined and vertical cracks were developed in several locations in the specimen (Fig. 7). This

304 was because of the inadequate lateral tensile strength of the RPC jacket, which was not able to

305 resist the expansion of the concrete core. The ultimate axial load of Specimen CJ-0 was only 6%

306 higher than the yield axial load as the confinement of the RPC jacket on the concrete core was

307 not significant. After reaching the ultimate axial load, the axial load dropped to about 80% of the

308 ultimate axial load due to the vertical splitting in the RPC jacket. This was followed by a

309 softening phase, as the RPC jacket did not entirely fail. Later, the axial load dropped to about

310 55% of the ultimate axial load due to the inclined splitting in the RPC jacket. Afterwards, the

311 confinement provided by the steel helices prevented further expansion of the concrete core and

312 the specimen showed a decrease in the axial load with the increase in the axial deformation

313 (softening response). The final failure occurred when some parts of the RPC jacket were

314 separated from the body of the specimen (Fig. 7). Specimens CJ-0 had a gradual failure during

315 the test and the concrete core of the specimen demonstrated resistance and integrity up to the end

316 of the test. Axial deformation of Specimens CJ-0 at failure was 21 mm, which was about 10%

317 higher than the axial deformation of Specimen C-0 at failure. Specimen CJ-0 achieved a

318 significant enhancement in the axial load capacity with a yield strengthening ratio of 2.78 and an

319 ultimate strengthening ratio of 2.55 (Table 5). The ductility of Specimen CJ-0 was 1.4, which is

320 less than the ductility of Specimen C-0. This can be attributed to the considerable enhancement

321 in the axial stiffness due to the RPC jacket, which decreased the deformability and thereby

322 decreased the ductility. Nevertheless, the energy absorption ratio of Specimen CJ-0 was 1.6.

323

324 Specimen CJF-0 failed by the rupture of the CFRP at the upper one-third segment of the

325 specimen followed by crushing of RPC jacket (Fig. 7). The axial load of the specimen increased

326 up to the ultimate axial load due to the wrapping of the CFRP. Afterwards, a drop in the axial

327 load occurred due to the rupture of the CFRP, which decreased the axial load to about 75% of the

328 ultimate axial load. The subsequent drop in the axial load decreased the axial load to about 50%

329 of the ultimate axial load, which occurred due to the crushing in the RPC jacket. This was

330 followed by a ductile behaviour with softening response due to the confinement of the steel

331 helices up to the end of the test. The test was stopped when the axial deformation of Specimen

332 CJF-0 reached to 25 mm. It is noted that Specimen CJF-0 did not entirely fail at the axial

333 deformation of 25 mm. Specimen CJF-0 had a yield strengthening ratio and an ultimate

334 strengthening ratio of 3.69 and 3.4, respectively. The ductility of Specimen CJF-0 was 1.8 and

335 the energy absorption ratio was 3.07 (Table 5).

336

337 It is apparent that Specimens CJ-0 and CJF-0 had higher ultimate axial load and energy

338 absorption capacity than Specimen CF-0. In addition, the yield strengthening ratio of Specimens

339 CJ-0 and CJF-0 was 109% and 177%, respectively, higher than the yield strengthening ratio of

340 Specimen CF-0. This indicates that the strengthening of circular RC columns with RPC and RPC

341 plus CFRP is more effective than strengthening with CFRP only to achieve a higher yield

342 strength. This can be explained by the fact that confinement has a marginal beneficial effect on

343 the yield strength. Furthermore, the ductility of Specimen CJF-0 was 28% higher than the

344 ductility of Specimen CJ-0 and energy absorption of Specimen CJF-0 was 92% greater than

345 energy absorption of Specimen CJ-0. Wrapping of the RPC jacket for Specimen CJF-0 not only

346 increased the ultimate axial load and the ductility but also prevented the expansion of the

347 concrete core, which was the major cause of the failure of Specimen CJ-0.

348

349 *3.3 Behaviour of the eccentrically loaded specimens*

350 Axial load-axial deformation response of the specimens tested under eccentric axial load with 15

351 mm eccentricity is shown in Fig. 8. Specimen C-15 failed by outward buckling and tensile

352 cracks at the tension side followed by the crushing of concrete at the compression side, as shown

353 in Fig. 9. The yield axial load of Specimen C-15 was 393 kN and the yield axial deformation was

354 2.2 mm. Specimen C-15 achieved an ultimate axial load of 436 kN, which was followed by a

355 softening response. The ductility of Specimen C-15 was 1.9, which was achieved due to the

356 confinement provided by the transverse reinforcement. The energy absorption of Specimen C-15

357 was 2057 kN.mm (Table 6).

358

359 Specimen CF-15 failed initially by outward buckling on the tension face and later by rupture of

360 the CFRP with crushing of concrete on the compression face at the mid-height of the specimen.

361 Specimen CF-15 exhibited initial axial load-axial deformation behaviour similar to that of

362 Specimen C-15. However, the yield strengthening ratio of Specimen CF-15 was 1.18 and the

363 ultimate strengthening ratio was 1.31. Specimen CF-15 achieved a higher ductility than

16

364   Specimen C-15. The ductility and energy absorption ratio of Specimen CF-15 were 4.3 and 2,

365   respectively (Table 6).

366

367   The failure of Specimen CJ-15 occurred by tensile-flexural cracking with splitting vertical cracks

368   at the upper one-third segment of the specimen, as shown in Fig. 9. The axial load of Specimen

369   CJ-15 increased up to the ultimate axial load then dropped to about 50% of the ultimate axial

370   load due to the splitting of the RPC jacket. Later the specimen showed a softening response due

371   to the confinement provided by the internal steel helices. Specimen CJ-15 achieved a higher

372   yield strengthening ratio and a higher ultimate strengthening ratio than Specimen CF-15. The

373   specimen achieved a yield strengthening ratio of 3.72 and an ultimate strengthening ratio of 3.53.

374   The ductility of Specimen CJ-15 was 1.3 and the energy absorption ratio was 3.73 (Table 6).

375

376   Specimen CJF-15 failed by the rupture of CFRP and the crushing of concrete at the mid-height

377   of the specimen at the compression side (Fig. 9). General axial load-axial deformation behaviour

378   of Specimen CJF-15 was similar to that of Specimen CJ-15. However, Specimen CJF-15

379   achieved higher yield axial load, ultimate axial load, axial ductility and energy absorption

380   compared to Specimen CJ-15. The yield strengthening ratio of Specimen CJF-15 was 3.95 and

381   the ultimate strengthening ratio was 4.07. The ductility and the energy absorption ratio of

382   Specimen CJF-15 were 1.4 and 4.5, respectively (Table 6).

383

384   Figure 10 shows the axial load-axial deformation response of the specimens tested under the

385   eccentric axial load of 25 mm eccentricity. Specimen C-25 failed by the crushing of concrete at

386   the mid-height segment of the specimen followed by concrete cracking on the tension face at the

17

387 upper one-third segment of the specimen (Fig. 11). The axial load-axial deformation response of

388 Specimen C-25 was characterized by a yield axial load of 295 kN with a yield axial deformation

389 of 2.6 mm and an ultimate axial load of 338 kN. The ultimate axial load was followed by a

390 softening response. The ductility and energy absorption of Specimen C-25 were 2.3 and 1916

391 kN.mm, respectively (Table 7).

392

393 The failure of Specimen CF-25 occurred by outward buckling at the tension face then by

394 rupturing of CFRP and crushing of concrete at the compression face, as shown in Fig. 11. The

395 axial load of Specimen CF-25 gradually increased up to the ultimate axial load, which was

396 followed by a softening response up to the final failure , which occurred by the rupture of CFRP.

397 Specimen CF-25 achieved a yield strengthening ratio of 1.33 and an ultimate strengthening ratio

398 of 1.41. The ductility of Specimen CF-25 was 3.5 and the energy absorption ratio was 2.1 (Table

399 7).

400

401 Specimen CJ-25 failed by typical tensile-flexural failure at the mid-height segment of the

402 specimen with crushing and splitting of RPC, as shown in Fig. 11. Specimen CJ-25 achieved

403 ultimate axial load of 1276 kN then the axial load dropped to about 45% of the ultimate axial

404 load. Afterwards, the specimen exhibited a softening response due to the confinement provided

405 by the internal lateral steel reinforcement. For Specimen CJ-25, the yield strengthening ratio was

406 3.92 and the ultimate strengthening ratio was 3.77. Ductility of Specimen CJ-25 was 1.2 and

407 energy absorption ratio was 2.3 (Table 7).

408

409   Specimen CJF-25 failed by the rupture of the CFRP and the crushing of the RPC at the upper

410   one-third segment of the specimen (Fig. 11). The initial axial load-axial deformation response of

411   Specimen CJF-25 was similar to that of Specimen CJ-25. However, Specimen CJF-25

412   demonstrated higher yield strengthening ratio, ultimate strengthening ratio, ductility and energy

413   absorption ratio compared to Specimen CJ-25. The yield strengthening ratio of Specimen CJF-25

414   was 4.34 and the ultimate strengthening ratio was 4.05. Ductility of Specimen CJF-25 was 1.5

415   and energy absorption ratio was 3.17 (Table 7).

416

417   *3.4. Behaviour of the specimens under four-point bending*

418   The flexural load-midspan deflection curves of the specimens tested under four-point bending

419   are shown in Fig. 12. All the specimens tested under four-point bending failed by typical vertical

420   flexural cracks at the midspan region of the specimen, as shown in Fig. 13. Initially, the first

421   vertical crack was formed then the crack became wider when the applied load reached the

422   ultimate load. Several cracks were observed after the ultimate load. All the cracks started from

423   the tension side of the specimen and propagated upwards within the midspan region of the

424   specimen.

425

426   Initial load-midspan deflection response of Specimen C-B was quasi-linear with a yield load of

427   115 kN and corresponding yield deflection of 7.7 mm. Afterward, the flexural load-midspan

428   deflection response showed a slightly hardening response up to the ultimate flexural load of 157

429   kN with the corresponding deflection of 53 mm. The final failure of the specimen occurred

430   suddenly by the rupture of the farthest tensile steel bar at the midspan deflection of 64 mm.

431   Specimen C-B achieved a high ductility of 8.3 and an energy absorption of 8530 kN.mm (Table

19

432 8). The high ductility of Specimen C-B was due to the high ultimate tensile strength of the steel

433 bars.

434

435 The initial part of the load-midspan deflection curve of Specimen CF-B was similar to that of

436 Specimen C-B. However, Specimen CF-B showed a steeper hardening response after the yield

437 load of 156 kN. Immediately after the ultimate load of 212 kN, the load dropped suddenly due to

438 wide cracks that formed between the CFRP strips in the midspan region at the tension side of the

439 specimen. Both the yield strengthening ratio and the ultimate strengthening ratio of Specimen

440 CF-B was 1.35. The ductility of Specimen CF-B was 4.1 and the energy absorption ratio was

441 0.95. The low energy absorption ratio of Specimen CF-B was due to the sudden failure of the

442 specimen after the ultimate load (Fig. 12).

443

444 The initial flexural load-midspan deflection response of Specimen CJ-B was steeper than the

445 flexural load-midspan deflection response of Specimens C-B and CF-B. The initial steeper

446 flexural load-midspan deflection response of Specimen CJ-B represented the higher initial

447 effective stiffness of Specimen CJ-B. After the ultimate flexural load, the flexural load-midspan

448 deflection showed a softening response until the final failure which occurred by a wide crack at

449 the tension side and crushing of RPC at the compression side. The yield strengthening ratio and

450 ultimate strengthening ratio of Specimen CJ-B were 2 and 1.89, respectively. Specimen CJ-B

451 achieved a flexural ductility of 3.8 with an energy absorption ratio of 1.06 (Table 8).

452

453 The initial flexural load-deflection response of Specimen CJF-B was close to that of Specimen

454 CJ-B. However, Specimen CJF-B achieved higher ultimate flexural load, ductility and energy

455   absorption than Specimen CJ-B due to the confinement effect of CFRP. The ultimate flexural

456   load of Specimen CJF-B was only 5% higher than the ultimate flexural load of Specimen CJ-B.

457   Specimen CJF-B failed by wide vertical cracks at the tension side and rupture of CFRP at the

458   compression side. The yield strengthening ratio of Specimen CJF-B was 2.2 and the ultimate

459   strengthening was 1.99. Specimen CJF-B exhibited a flexural ductility of 9.7 and an energy

460   absorption ratio of 1.38 (Table 8).

461

462   *3.5 Experimental axial load-bending moment interaction diagram*

463   The axial load-bending moment interaction diagrams for the four groups of specimens are

464   presented in Fig. 14. The axial load-bending moment interaction diagrams are drawn based on

465   the four experimental points obtained for each group of specimens in this study. The first point

466   represents the pure axial load. The second and the third points represent the axial loads and

467   bending moments at axial load eccentricities of 15 mm and 25 mm, respectively. The last point

468   represents the bending moment obtained from four-point bending test. The bending moments for

469   the specimens under eccentric axial loads were calculated by using Eq. (1). The bending moment

470   under four-point bending was calculated by using Eq. (2).

471

$$M \;=\; P(e + \delta) \tag{1}$$

$$M = \frac{PL}{6} \tag{2}$$

472

473   where M is the bending moment, P is the ultimate load, e is the eccentricity, δ is the midspan

474   lateral deformation at the corresponding ultimate axial load and L is the span length of the

475   specimen, which was 700 mm in this study.

21

476 The experimental axial load-bending moment interaction showed the superior performance of the

477 Groups CJ and CJF specimens compared to Groups C and CF specimens. Group CJ specimens

478 obtained greater ultimate axial load than Groups C and CF specimens under concentric axial

479 load, 15 mm eccentric axial load and 25 mm eccentric axial load. In addition, Group CJF

480 specimens achieved higher ultimate axial load than Group CJ specimens under concentric and

481 eccentric axial loading. Similarly, Group CJ specimens obtained greater bending moment than

482 Groups C and CF specimens under 15 mm eccentric axial load, 25 mm eccentric axial load and

483 under four-point bending. Group CJF specimens achieved higher bending moment than Group

484 CJ specimens under 15 mm eccentric axial load, 25 mm eccentric axial load and four-point

485 bending. Table 9 presents the results of the axial-load bending moment interactions. For the

486 eccentric axial load with the eccentricity of 15 mm, bending moments of Groups CF, CJ and CJF

487 were 126%, 213% and 278%, respectively, higher than the bending moment of Group C. For the

488 eccentric axial load with the eccentricity of 25 mm, bending moments of Groups CF, CJ and CJF

489 were 84%, 208% and 238%, respectively, higher than the bending moment of Group C. Under

490 four-point bending, the bending moments for Groups CF, CJ and CJF were 39%, 94% and 100%,

491 respectively, higher than the bending moment of Group C.

492

493 Based on the above experimental results, it is apparent that jacketing with RPC only (without

494 FRP wrapping) can be used to increase the maximum axial and maximum flexural loads of

495 circular RC columns. Nevertheless, jacketing with RPC and FRP is recommended to achieve

496 higher structural ductility and energy absorption capacity together with improved maximum

497 axial load and maximum bending moment.

498

4. Conclusions

A new jacketing technique is proposed to retrofit existing deficient circular RC columns. The new jacketing technique consisted of jacketing the RC column with a thin layer of RPC then wrapping with CFRP. The behaviour of 16 RC column specimens under concentric axial load, eccentric axial loads and four-point bending was experimentally investigated. The load-deformation responses of the tested specimens under concentric axial load, eccentric axial loads as well as under four-point bending are presented. Also, ductility and energy absorption were calculated. Furthermore, the axial load-bending moment interaction diagrams for groups of the tested specimens are plotted. Based on the experimental results of the current study, the following conclusions can be drawn:

1. Under concentric axial load, eccentric axial loads and four-point bending, the yield and ultimate strengthening ratios of circular RC column specimens strengthened with RPC jacket were significantly higher than the yield and ultimate strengthening ratios, respectively, of the circular RC specimens strengthened with CFRP wrapping.

2. The specimens strengthened with CFRP wrapping achieved higher ductility compared to the specimens strengthened with RPC jacket. However, the specimens strengthened with RPC jacket achieved higher energy absorption ratios than the specimens strengthened with CFRP wrapping under concentric axial load, eccentric axial loads and four-point bending.

3. The ultimate strengthening ratios, ductility and the energy absorption ratios of circular RC specimens strengthened with RPC jacket and CFRP wrapping were higher than those of the circular RC specimens strengthened with RPC jacket under concentric axial load, eccentric axial loads and four-point bending.

522   4.   The proposed jacketing technique of the circular RC columns with RPC jacketing and FRP

523   wrapping was found to be an effective strengthening technique to increase the yield load,

524   ultimate load and energy absorption capacity of the existing inadequate circular RC

525   columns.

526

537

538   **References**

539   [1] S.P.B. Waghmare, Materials and jacketing technique for retrofitting of structures,

540   International Journal of Advanced Engineering Research and Studies, 1(1) (2011) 15-19.

541   [2] G. Campione, M. Fossetti, C. Giacchino, G. Minafò, RC columns externally strengthened

542   with RC jackets, Materials and Structures, 47(10) (2014) 1715-1728.

543   [3] E. Júlio, F. Branco, V. Silva, Structural rehabilitation of columns with reinforced concrete

544   jacketing, Progress in Structural Engineering and Materials, 5(1) (2003) 29-37.

545   [4] V. Marlapalle, P. Salunke, N. Gore, Analysis & design of RCC jacketing for buildings,

546   International Journal of Recent Technology and Engineering, 3 (2014) 62-63.

547   [5] H. Sezen, E.A. Miller, Experimental Evaluation of Axial Behaviour of Strengthened Circular

548   Reinforced-Concrete Columns, Journal of Bridge Engineering, 16(2) (2011) 238-247.

549   [6] Y.-F. Wu, T. Liu, D. Oehlers, Fundamental principles that govern retrofitting of reinforced

550   concrete columns by steel and FRP jacketing, Advances in Structural Engineering, 9(4) (2006)

551   507-533.

552   [7] V.M. Karbhari, Y. Gao, Composite jacketed concrete under uniaxial compression-

553   verification of simple design equations, Journal of materials in civil engineering, 9(4) (1997)

554   185-193.

555   [8] ACI 440.2R-17, Guide for the design and construction of externally bonded FRP systems for

556   strengthening concrete structures, American Concrete Institute, United States, 2017.

557   [9] M.N.S. Hadi, J. Li, External reinforcement of high strength concrete columns, Composite

558   Structures, 65(3) (2004) 279-287.

559   [10] M.N.S. Hadi, Behaviour of eccentric loading of FRP confined fibre steel reinforced concrete

560   columns, Construction and Building Materials, 23(2) (2009) 1102-1108.

561   [11] M.N.S. Hadi, T.M. Pham, X. Lei, New method of strengthening reinforced concrete square

562   columns by circularizing and wrapping with fibre-reinforced polymer or steel straps, Journal of

563   Composites for Construction, 17(2) (2013) 229-238.

564   [12] L. Lam, J. Teng, Design-oriented stress–strain model for FRP-confined concrete,

565   Construction and building materials, 17(6) (2003) 471-489.

566 [13] L.C. Bank, Composites for construction: Structural design with FRP materials, John Wiley

567 & Sons, 2006.

568 [14] P. Richard, M. Cheyrezy, Composition of reactive powder concretes, Cement and concrete

569 research, 25(7) (1995) 1501-1511.

570 [15] A. Sadrekarimi, Development of a light weight reactive powder concrete, Journal of

571 Advanced Concrete Technology, 2(3) (2004) 409-417.

572 [16] M.-G. Lee, Y.-C. Wang, C.-T. Chiu, A preliminary study of reactive powder concrete as a

573 new repair material, Construction and Building Materials, 21(1) (2007) 182-189.

574 [17] T. Chang, B. Chen, J. Wang, C. Wu, Performance of Reactive Powder Concrete (RPC) with

575 different curing conditions and its retrofitting effects on concrete member, In: Alexander et al

576 (Eds.), Concrete Repair, Rehabilitation and Retrofitting II, Taylor & Francis Group, London,

577 UK, 2009, pp. 1203-1208.

578 [18] A.R. Malik, S.J. Foster, Carbon fibre-reinforced polymer confined reactive powder concrete

579 columns-experimental investigation, ACI Structural Journal, 107(03) (2010) 263-271.

580 [19] L. Huynh, S. Foster, H. Valipour, R. Randall, High strength and reactive powder concrete

581 columns subjected to impact: Experimental investigation, Construction and Building Materials,

582 78 (2015) 153-171.

583 [20] AS 3972-2010, General purpose and blended cements, Australian Standards, Sydney, NSW,

584 2010.

585 [21] SIMCOA operations pty. ltd., Micro silica material safety data sheet,

586 http://www.simcoa.com.au/, 2016 (accessed 15.06.16).

26

587   [22] Australasian (iron & steel) Slag Association (ASA), Wollongong, NSW, Australia.

588   http://www.asa-inc.org.au/, 2016 (accessed 15.06.16).

589   [23]   BASF-Australia,   Master   Glenium®   SKY   8700-technical   data   sheet.

590   http://www.BASF.cam.au/, 2016 (accessed 15.06.16).

591   [24] Ganzhou Daye Metallic Fibres Co.,Ltd, Micro steel fibre WSF0213 III specifications.

592   http://www.gzdymf.com/, 2016 (accessed 15.06.16).

593   [25] Y. Ju, Y. Jia, H. Liu, J. Chen, Mesomechanism of steel fibre reinforcement and toughening

594   of reactive powder concrete, Science in China Series E: Technological Sciences, 50(6) (2007)

595   815-832.

596   [26] ASTM C230-14, Standard Specification for Flow Table for use in Tests of Hydraulic

597   Cement, American Society for Testing and Materials, West Conshohocken, PA, United States,

598   2014.

599   [27] AS 1012.9-2014, Compressive strength tests – concrete, mortar and grout specimen,

600   Australian Standards, Sydney, NSW, 2014.

601   [28] AS 1012.10-2014, Determination of indirect tensile strength of concrete cylinders,

602   Australian Standards, Sydney, NSW, 2014.

603   [29] AS 1012.11-2014, Determination of the modulus of rupture, Australian Standards, Sydney,

604   NSW, 2014.

605   [30] JS SF6-1999, Method of test for shear strength of steel fibre reinforced concrete, Japan

606   Society of Civil Engineers (JSCE), Tokyo, Japan, 1999.

607   [31] AS 3600-2009, Concrete Structures, Australian Standards, Sydney, NSW, 2009.

608   [32] AS 1391-2007, Metallic materials tensile testing at ambient temperatures, Australian

609   Standards, Sydney, NSW, 2007.

610   [33] ASTM D3039-08, Standard test method for tensile properties of polymer matrix composite

611   materials, American Society for Testing and Materials, West Conshohocken, PA, United States,

612   2008.

613   [34] M.N.S. Hadi, F. Alhussainy, M.N. Sheikh, Behaviour of self-compacting concrete columns

614   reinforced longitudinally with steel tubes, Journal of Structural Engineering, 143(6) (2017)

615   04017024.

616   [35] M.N.S. Hadi, H.A. Hasan, M.N. Sheikh, Experimental Investigation of Circular High-

617   Strength Concrete Columns Reinforced with Glass Fibre-Reinforced Polymer Bars and Helices

618   under Different Loading Conditions, Journal of Composites for Construction, 21(4) (2017)

619   04017005.

620   [36] S. Pessiki, A. Pieroni, Axial load behaviour of large-scale spirally-reinforced high-strength

621   concrete columns, ACI Structural journal, 94(3) (1997) 304-314.

622   [37] M.N.S. Hadi, Q.S. Khan, M.N. Sheikh, Axial and flexural behaviour of unreinforced and

623   FRP bar reinforced circular concrete filled FRP tube columns, Construction and Building

624   Materials, 122 (2016) 43-53.

625   [38] ASTM C1018-97, Flexural Toughness and First-Crack Strength of Fibre-reinforced

626   Concrete (Using Beam with Third-Point Loading), American Society for Testing and Materials,

627   West Conshohocken, PA, United States, 1997.

628

629

642

643

644

645

List of Figures

667

668

Table 1

Test matrix

Specimen	Dimensions (mm)	Longitudinal reinforcement	Transverse reinforcement	Jacket type	Loading condition
C-0	Ø150 × 800	6N10	R6@50 mm	None	Concentric
C-15					15 mm eccentric
C-25					25 mm eccentric
C-B					Four-point bending
CF-0	Ø150 × 800			Two layers of CFRP	Concentric
CF-15					15 mm eccentric
CF-25					25 mm eccentric
CF-B					Four-point bending
CJ-0	Ø200 × 800			RPC	Concentric
CJ-15					15 mm eccentric
CJ-25					25 mm eccentric
CJ-B					Four-point bending
CJF-0	Ø200 × 800			RPC + One layer of CFRP	Concentric
CJF-15					15 mm eccentric
CJF-25					25 mm eccentric
CJF-B					Four-point bending

671

672

31

673

Table 2

Components of RPC mix

Components kg/m^3 (by cement mass)					
Cement	Silica fume	River sand (150-600) µm	Superplasticizer	Water	Steel fibre 13 mm length
880 (1.00)	220 (0.25)	924 (1.05)	50.16 (0.057)	176 (0.20)	117 (0.13)

676

677

678

679

680

Table 3

Mechanical properties of the RPC on the 28th day

Property	Specimen type	Specimen Dimensions (mm)	Test result
Compressive strength (MPa)	Cylinder	100×200	110
Splitting tensile strength (MPa)	Cylinder	150×300	9
Modulus of rupture (MPa)	Prism	100×100×500	12
Shear strength (MPa)	Prism	150×150×500	30

683

684

685

686

687

688 **Table 4**

689   Properties of the CFRP sheets

Property	Number of layers	
	1	2
Average Width (mm)	25	25
Average maximum tensile strain (mm/mm)	0.0186	0.0247
Average tensile modulus per unit width (N/mm)	28871	50567
Average maximum tensile force per unit width (N/mm)	537	1249

690

691

692

693

694

Table 5

Experimental results of specimens tested under concentric axial load

Specimen	C-0	CF-0	CJ-0	CJF-0
Yield axial load (kN)	536	714	1490	1977
Axial deformation at yield axial load (mm)	2. 9	4.5	2.4	3.4
Ultimate axial load (kN)	615	1245	1573	2094
Axial deformation at ultimate axial load (mm)	4.5	17.6	2.7	6
Yield strengthening ratio	1	1.33	2.78	3.69
Ultimate strengthening ratio	1	2.02	2.55	3.4
Ductility	5.7	4	1.4	1.8
Energy absorption (kN.mm)	4297	6165	6867	13221
Energy absorption ratio	1	1.43	1.6	3.07

697

698

699

700

Table 6

Experimental results of specimens tested under eccentric axial load (eccentricity = 15 mm)

Specimen	C-15	CF-15	CJ-15	CJF-15
Yield axial load (kN)	393	465	1463	1554
Axial deformation at yield axial load (mm)	2.2	3	3.5	3.5
Ultimate axial load (kN)	436	572	1542	1777
Axial deformation at ultimate axial load (mm)	2.9	8.2	3.8	4.8
Yield strengthening ratio	1	1.18	3.72	3.95
Ultimate strengthening ratio	1	1.31	3.53	4.07
Ductility	1.9	4.3	1.3	1.4
Energy absorption (kN.mm)	2057	4108	7683	9273
Energy absorption ratio	1	2	3.73	4.5

703

704

705

706

707

Table 7

Experimental results of specimens tested under eccentric axial load (eccentricity = 25 mm)

Specimen	C-25	CF-25	CJ-25	CJF-25
Yield axial load (kN)	295	393	1158	1282
Axial deformation at yield axial load (mm)	2.6	3.6	2.8	3
Ultimate axial load (kN)	338	478	1276	1371
Axial deformation at ultimate axial load (mm)	3.8	8	3	4
Yield strengthening ratio	1	1.33	3.92	4.34
Ultimate strengthening ratio	1	1.41	3.77	4.05
Ductility	2.3	3.5	1.2	1.5
Energy absorption (kN.mm)	1916	4025	4424	6085
Energy absorption ratio	1	2.1	2.3	3.17

710

711

712

713

714

Table 8

Experimental results of specimens tested under four-point bending

Specimen	C-B	CF-B	CJ-B	CJF-B
Yield flexural load (kN)	115	156	230	254
Deflection at yield flexural load (mm)	7.7	11.7	3.9	4
Ultimate flexural load (kN)	157	212	298	313
Deflection at ultimate flexural load (mm)	53	40	10	18
Yield strengthening ratio	1	1.35	2	2.2
Ultimate strengthening ratio	1	1.35	1.89	1.99
Ductility	8.3	4.1	3.8	9.7
Energy absorption (kN.mm)	8530	8100	9061	11787
Energy absorption ratio	1	0.95	1.06	1.38

717

718

719

720

721

Table 9

Experimental axial load-bending moment interactions

Specimen	Ultimate load (kN)	Lateral deformation at ultimate axial load	Ultimate bending moment (kN.m)
C-0	615	-	-
C-15	436	3.7	8.1
C-25	338	7	10.8
C-B	157	-	18
CF-0	1245	-	-
CF-15	572	17	18.3
CF-25	478	16.6	19.9
CF-B	212	-	25
CJ-0	1573	-	-
CJ-15	1542	1.5	25.4
CJ-25	1276	1.1	33.3
CJ-B	298	-	35
CJF-0	2094	-	-
CJF-15	1777	2.2	30.6
CJF-25	1371	1.6	36.5
CJF-B	313	-	36

724

725
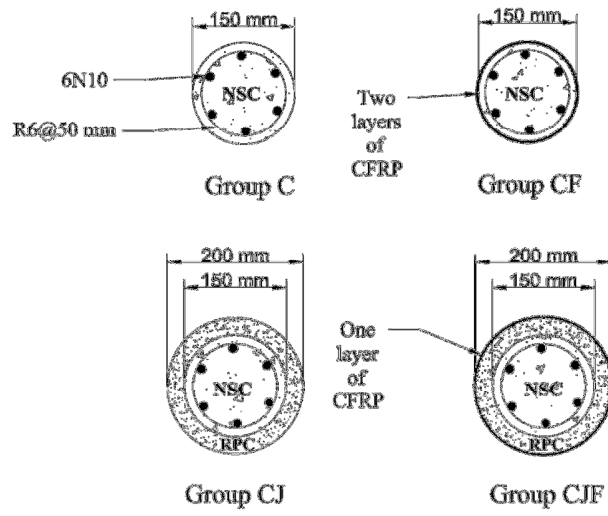
Fig. 1. Plan view of the reference and the strengthened specimens

726

727

728

729

730

731

732

733

734

735

736

737

738

739

740

741

742

743

744

745

746

747

748

749

750

751

752

753

754

755

756

757

758

759

760

761

762

763

764

Fig. 2. Steel fibres

765

766

767

768

769

770

771

772

773

774

775

Chamber

Sandblasting accessories

Chipping hammer

(a)   (b)

776   **Fig. 3.** Preparation of surface of base specimen: (a) sandblasting chamber with accessories and

777   (b) use of chipping hammer

778

779

780

781

782

783

784

785

786

787

788

789

790   (a)   (b)   (c)

791   **Fig. 4.** Formworks of the base and jackted specimens: (a) formwork of base specimen, (b)

792   formwork of jackted specimen and (c) jacketed specimen after casting

793

794

795

796

797

798

799

800

801

802   Loading heads

803

804

805

806
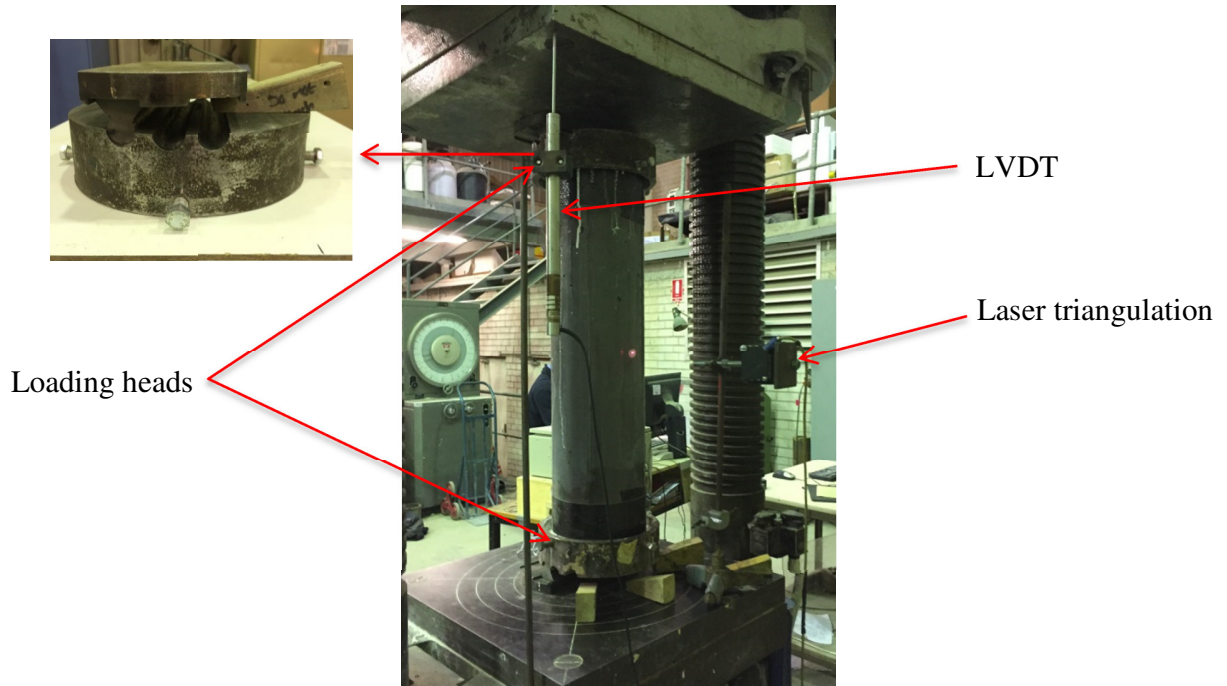
807   **Fig. 5.** Test setup of eccentrically loaded specimen

808

809

810

LVDT

Laser triangulation

811

812
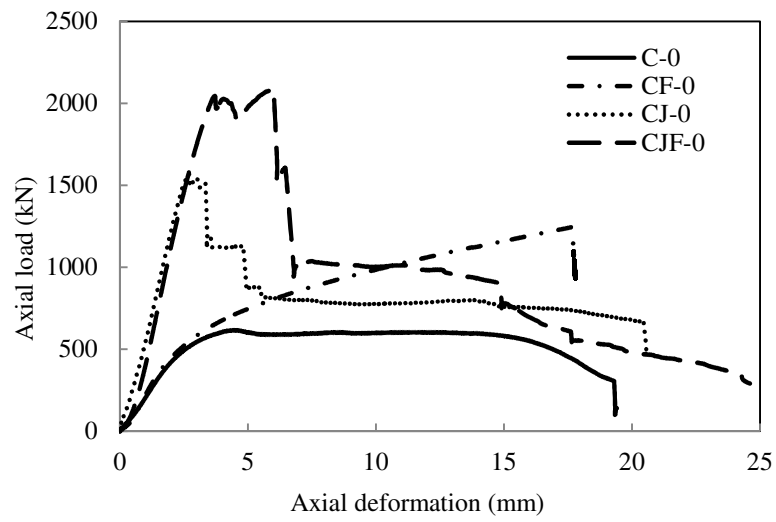
Fig. 6. Axial load-axial deformation responses of the specimens tested under concentric axial

load

815

816

817

818

819

Fig. 7. Failure modes of the specimens tested under concentric axial load

828
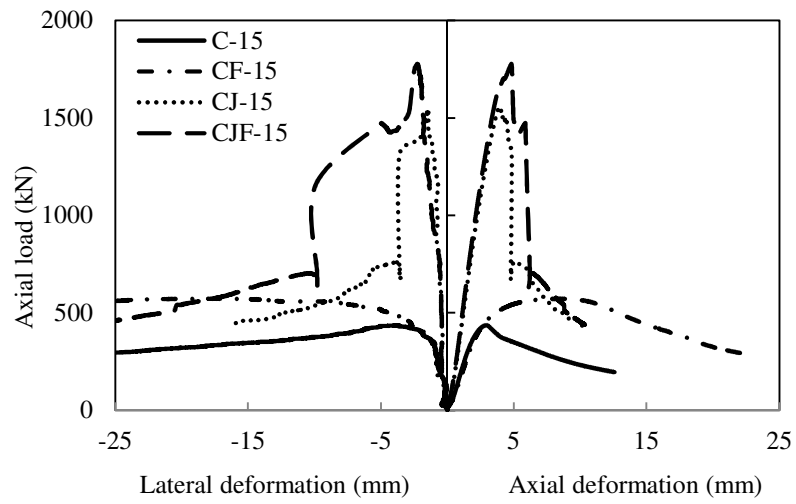
829

830   **Fig. 8.** Axial load-axial deformation and axial load-lateral deformation responses of the

831   specimens tested under eccentric axial load (eccentricity = 15 mm)

832

833

834

835

836

837

838

839

840   **Fig. 9.** Failure modes of the specimens tested under eccentric axial load (eccentricity = 15 mm)
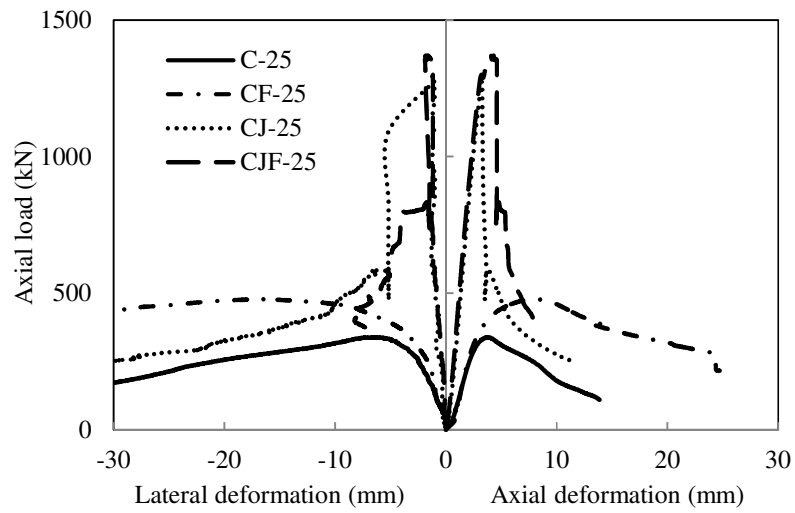
841

842

843

844

845

846

847

Fig. 10. Axial load-axial deformation and axial load-lateral deformation responses of the

specimens tested under eccentric axial load (eccentricity = 25 mm)

850

851

852

853

854

855

856

857 **Fig. 11.** Failure modes of the specimens tested under eccentric axial load (eccentricity = 25 mm)
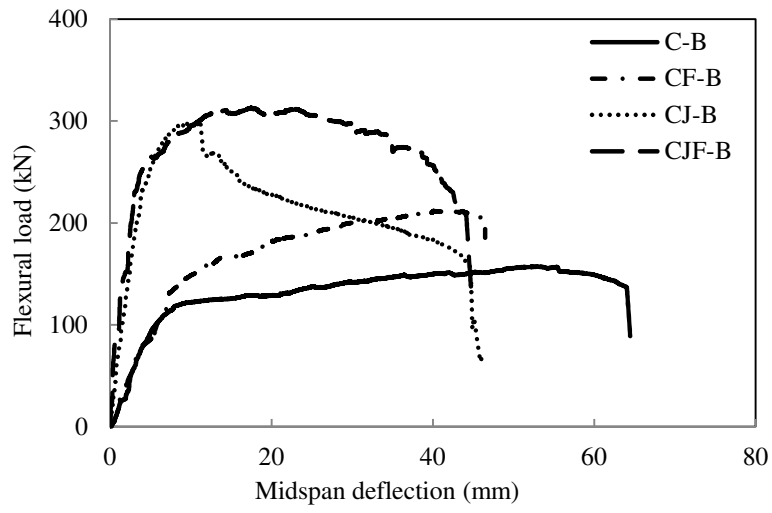
858

859

860

861

862

863

864

865 **Fig. 12.** Flexural load-midspan deflection curves of the specimens tested under four-point

866 bending

867

868

869

870

871

872

Fig. 13. Failure modes of the specimens tested under four-point bending
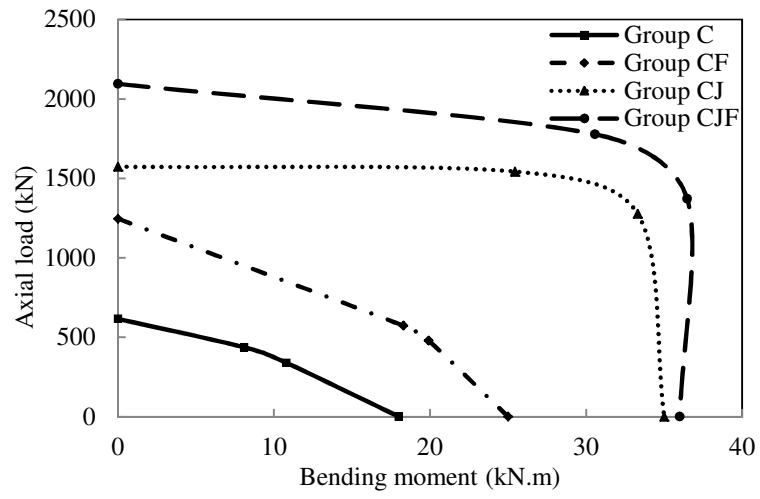
874

875

876

877

878

879

880

881 **Fig. 14.** Experimental axial load-bending moment interaction diagrams

882

883